Earth and Planetary Science Letters 547 (2020) 116447

Contents lists available at ScienceDirect

Earth and Planetary Science Letters

www.elsevier.com/locate/epsl

In search for the missing arc root of the Southern California Batholith: P-T-t evolution of upper mantle xenoliths of the Colorado Plateau Transition Zone

Ojashvi Rautela [a,*], Alan D. Chapman [a], Jessie E. Shields [b], Mihai N. Ducea [c,d], Cin-Ty Lee [e], Hehe Jiang [e], Jason Saleeby [f]

[a] Geology Department, Macalester College, St. Paul, MN 55105, USA
[b] Department of Earth and Environmental Sciences, California State University, Fresno, CA 93740, USA
[c] Department of Geosciences, University of Arizona, Tucson, AZ 85721, USA
[d] Faculty of Geology and Geophysics, University of Bucharest, 010041 Bucharest, Romania
[e] Department of Earth Science, Rice University, Houston, TX 77005, USA
[f] Division of Geological and Planetary Sciences, California Institute of Technology, Pasadena, CA 91125, USA

ARTICLE INFO

Article history:
Received 13 January 2020
Received in revised form 24 June 2020
Accepted 28 June 2020
Available online xxxx
Editor: A. Yin

Keywords:
Laramide
Colorado Plateau Transition Zone
Southern California Batholith
Cordilleran tectonics
garnet-clinopyroxenite
P-T-t evolution

ABSTRACT

Xenolith and seismic studies provide evidence for tectonic erosion and eastward displacement of lower crust-subcontinental mantle lithosphere (LC-SCML) underlying the Mojave Desert Region (i.e. southern California batholith (SCB)). Intensified traction associated with the Late Cretaceous flattening of the subducting Farallon plate, responsible for deforming the SW U.S., likely played a key role in "bulldozing" the tectonically eroded LC-SCML ~500 km eastwards, to underneath the Colorado Plateau Transition Zone (CPTZ) and further inboard. The garnet clinopyroxenite xenoliths from two CPTZ localities, Chino Valley and Camp Creek (central Arizona), provide a rare glimpse of the material underlying the CPTZ. Thermodynamic modeling, in addition to major and trace element thermobarometry, suggests that the xenoliths experienced peak conditions of equilibration at 600-900 °C and 12-28 kbar. These peak conditions, along with the composition of the xenoliths (type "B" garnet and diopsidic clinopyroxene) strongly suggest a continental arc residue ("arclogite"), rather than a lower plate subduction ("eclogite"), origin. A bimodal zircon U-Pb age distribution with peaks at ca. 75 and 150 Ma, and a Jurassic Sm-Nd garnet age (154 ± 16 Ma, with initial εNd value of +8) overlaps eastern SCB pluton ages and suggests a consanguineous relationship. Cenozoic zircon U-Pb ages, REE geochemistry of zircon grains, and partially re-equilibrated Sm-Nd garnet ages indicate that displaced arclogite remained at elevated PT conditions (>700 °C) for 10s of Myr following its dispersal until late Oligocene entrainment in host latite. With a ~100 Myr long thermal history overlapping that of the SCB and the CPTZ, these assemblages also contain evidence for late-stage hydration (e.g. secondary amphibole), potentially driven by de-watering of the Laramide slab.

In light of these results, we suggest that the CPTZ arclogite originates from beneath the eastern half of the SCB, where it began forming in Late Jurassic time as mafic keel to continental arc magmas. The displacement and re-affixation of the arclogites further inboard during the Late Cretaceous flat slab subduction, might have contributed to the tectonic stability of the Colorado Plateau relative to adjacent geologic provinces through Laramide time and likely preconditioned the region to Cenozoic tectonism, e.g. present-day delamination beneath the plateau, high-magnitude extension and formation of metamorphic core complexes.

1. Introduction

The Late Cretaceous-early Paleogene Laramide Orogeny resulted in deformation of the southwest North American craton edge. A plate tectonic trigger for the orogeny is intensified traction and tectonic erosion of the lower crust-subcontinental mantle lithosphere

* Corresponding author at: Division of Geological and Planetary Sciences, California Institute of Technology, Pasadena, CA 91125, USA.
E-mail address: orautela@caltech.edu (O. Rautela).

https://doi.org/10.1016/j.epsl.2020.116447
0012-821X/

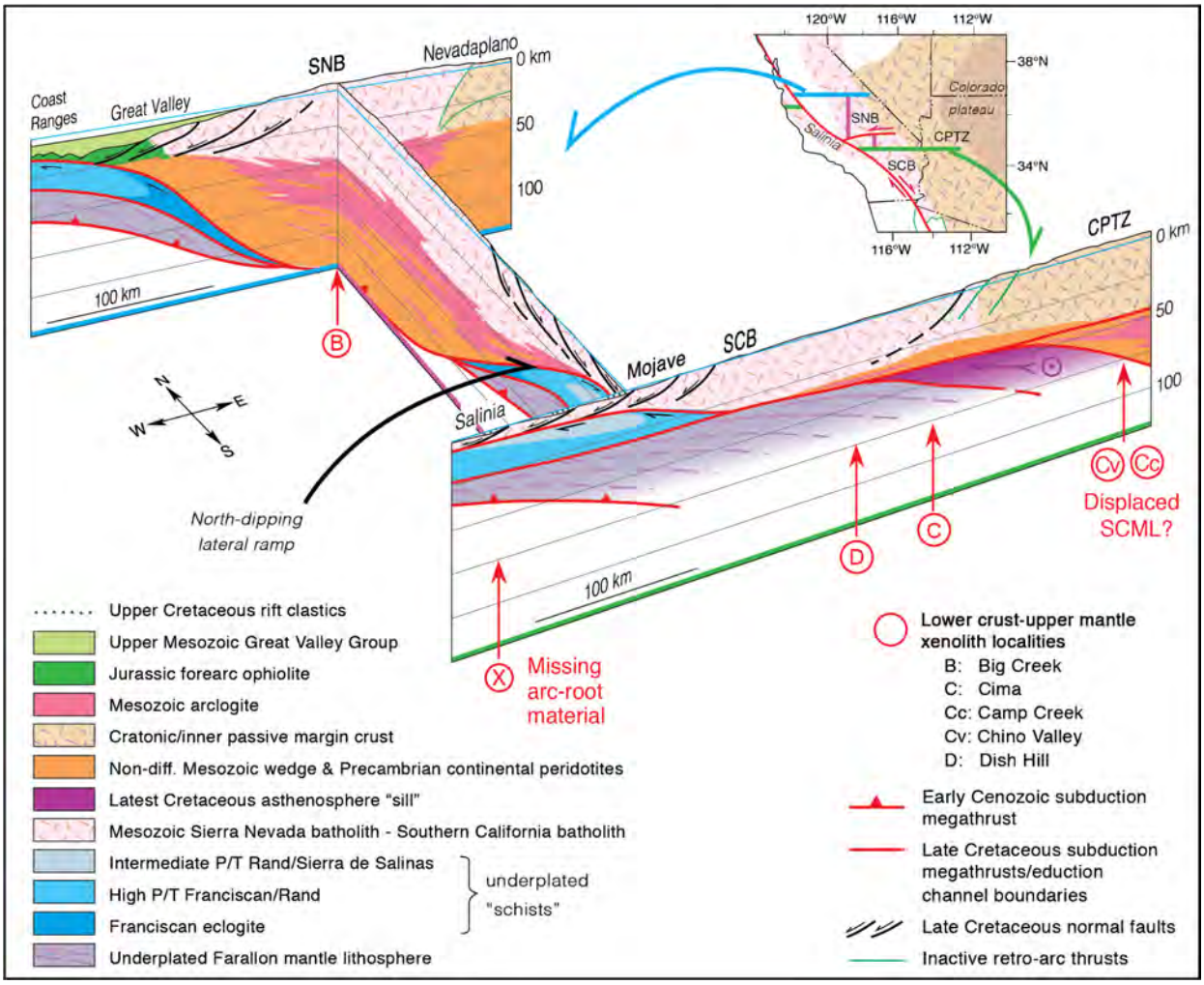

Fig. 1. Fence diagram showing idealized lithospheric structure for beginning of Cenozoic time. Parallel sections across Sierra Nevada batholith (SNB) - Great Valley forearc and southern California batholith (SCB) - Colorado Plateau transition zone (CPTZ), and a linking section across the southern Sierra subduction megathrust lateral ramp. Locations of the sections shown on inset. Note the position of missing arc-root (marked by X) and hypothesized location of displaced LC-SCML (orange and pink) in the SCB cross section. Modified from Chapman et al. (2020). (For interpretation of the colors in the figure the reader is referred to the web version of this article.)

(LC-SCML) as a response to unusually shallow and flat-slab subduction of the Farallon plate (Livaccari et al., 1981; Bird, 1988; Saleeby, 2003; Liu et al., 2010). The principal plate edge damage zone associated with the orogeny consists of the ~500 km long Laramide deformation corridor — the southern California batholith (SCB), lying primarily in the Mojave Desert region, and the southernmost Sierra Nevada Batholith (SNB). In contrast to the SNB to the north and the Peninsular Ranges batholith to the south, much of the SCB is rootless. Structural and petrologic relations preserved in the SCB and southernmost SNB indicate that the base of the batholith and underlying LC-SCML was sheared off at 30-35 km depths and underplated by subduction accretion assemblages (e.g. Rand and San Emigdio schists in the Mojave Region) that were transported inboard by shallow subduction (Jacobson et al., 1988; Barth et al., 2008; Grove et al., 2003; Saleeby, 2003; Luffi et al., 2009; Chapman et al., 2012; Ducea and Chapman, 2018; Chapman et al., 2019, 2020).

In this study, we focus on the tectonic evolution of the SW Cordillera LC-SCML, specifically the fate of the missing sub-SCB LC-SCML, by integrating new and existing (e.g. Esperanca et al., 1988; Smith et al., 1994; Erdman et al., 2016) petrogenetic and geo-thermochronologic studies of LC-SCML xenoliths. We assess the hypothesis that the shallow-angle subduction episode responsible for Laramide deformation, also "bulldozed" the SCB LC-SCML fragment ~500 km to the east and re-affixed (e.g. Axen et al., 2018; Chapman et al., 2019, 2020) it under the Colorado Plateau Transition Zone (CPTZ) in central Arizona (Fig. 1). This displaced LC-SCML fragment might also provide an intriguing explanation for the strength of the Colorado Plateau relative to adjacent geologic provinces (e.g., Morgan and Swanberg, 1985; Bashir et al., 2011; Erdman et al., 2016) and may have also preconditioned the region to Cenozoic tectonism, e.g. high-magnitude extension and formation of metamorphic core complexes and delamination beneath the plateau (e.g., Levander et al., 2011; Erdman et al., 2016; Chapman et al., 2019, 2020).

Lower crust and upper mantle xenoliths erupted within ca. 25 Ma Sullivan Buttes Latite (e.g., Arculus and Smith, 1979) in Chino Valley and correlative latite at Camp Creek, both exposed in central Arizona (detailed field observations in Chapman et al. (2020) Supplement), provide a rare glimpse of the deep lithosphere underlying the CPTZ (Fig. 1 and 2). If LC-SCML was indeed displaced eastwards from beneath the hot SCB (marked X in Fig. 1) to the colder craton interior (CPTZ) under similar lithospheric depths, the displaced material should record near isobaric cooling and contain an array of ages overlapping those of the SCB. In an effort to test the hypothesis delineated above, we constrain the pressure-temperature-time evolution of the sampled CPTZ xenoliths.

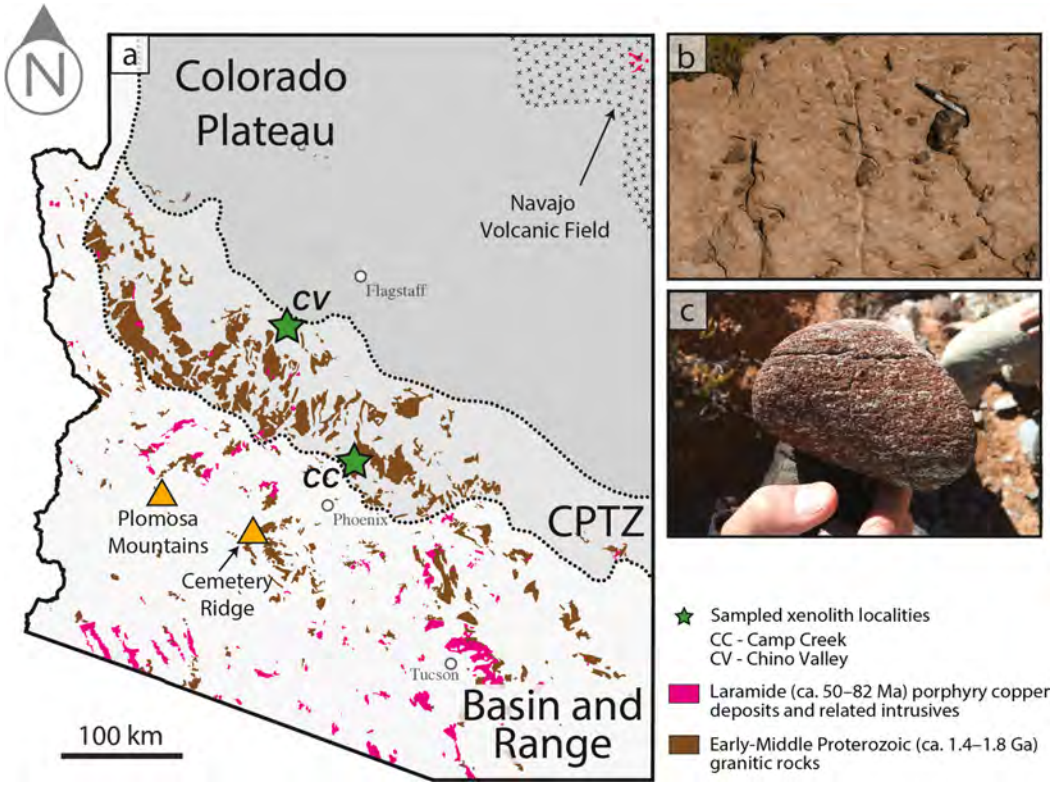

Fig. 2. Simplified geologic map and field images of the study region. (a) Simplified geologic map of Arizonan granite outcrops and sample locations (stars), modified from the Geologic Map of Arizona. Gray color from dark to light shades the physiographic provinces: the Colorado Plateau (dark), the Colorado Plateau Transition Zone (CPTZ), and the Basin and Range (light). (b) Block of lava latite hosting several smaller xenoliths (marker for scale); (c) Fist-sized hand sample of a rounded arclogite xenolith (finger for scale).

2. Background

2.1. SW Cordillera and the Laramide deformation

The deformation associated with the Laramide tectonics—westward breachment of the SCB segment of the Cordilleran batholith belt above the underplated schists—is much more geographically focused relative to the remainder of the Cordilleran margin (Saleeby, 2003). Plate kinematic reconstructions for the Pacific-Farallon ridge has led to the interpretation that the geographically restricted Laramide deformation resulted from the subduction of conjugate massifs to the Hess and Shatsky large igneous provinces, two oceanic plateaux residing in the SW Pacific (Livaccari et al., 1981; Liu et al., 2010). The initial impact of the Shatsky conjugate is consistent with evidence for widespread ductile thrusting within the SCB, deep crustal exhumation, shallow-angle tectonic underplating of schists (subduction accretionary assemblage), and - the focus of this paper— removal and displacement of the underlying LC-SCML (e.g. Saleeby, 2003; Luffi et al., 2009; Chapman et al., 2012, 2019, 2020).

The plate edge domain is underlain by trench assemblages (the Rand and related schists in the Mojave-southern Sierra Nevada-Salinia region) transported inboard by shallow-angle subduction (Jacobson et al., 1988; Grove et al., 2003; Porter et al., 2011; Chapman, 2017; Ducea and Chapman, 2018). These schists are exposed in the footwall of the shallowly dipping and regionally extensive Rand fault, interpreted as a remobilized subduction megathrust (e.g., Cheadle et al., 1986; Chapman, 2017), beneath deep crustal level SCB assemblages and the southern SNB (Fig. 1). These structural relations in the SCB and southernmost SNB indicate that the base of the batholith and underlying LC-SCML was sheared off at 30-35 km depth and replaced with trench sediments and fragments of Farallon lithosphere (Grove et al., 2003; Saleeby, 2003; Chapman, 2017). Despite the LC-SCML removal from beneath the SCB, and the subsequent tectonic underplating of schist, the base of the lithosphere in the Mojave region currently exceeds ~60 km depth (e.g. Luffi et al., 2009), implying that the mantle lithosphere beneath the schists was rebuilt in the latest Cretaceous-Cenozoic time.

2.2. Xenolith constraints on SW Cordillera LC-SCML

Colorado Plateau Region: The presence of Proterozoic upper mantle-lower crustal xenoliths within the Colorado Plateau, in conjunction with Nd isotopic data on widely dispersed mafic volcanic rocks (e.g. Livaccari and Perry, 1993) record the preservation of LC-SCML beneath the region through Laramide time. Lawsonite eclogitic xenoliths retrieved from the Four Corners region (Navajo Volcanic Field) of the Colorado Plateau (Fig. 2, Usui et al., 2003; Smith et al., 2004) suggest subduction underplating of Farallon mafic crust along the ancient ~100 km deep lithospheric lid (25-50 kbar conditions). The peridotites at Cemetery Ridge and Plomosa Mountains (Fig. 2) further point towards underlying fragments of forearc/arc mantle wedge (Haxel et al., 2014), perhaps transported inboard on the leading edge of the flat slab.

Mojave Desert Region: Geo-thermochronologic and isotopic signatures of peridotites from the Pliocene-Quaternary Cima cones suite (e.g. Lee et al., 2001) and the Quaternary Dish Hill cone (Luffi et al., 2009) in the east-central Mojave Desert (Fig. 1) are similar to those of nearby Precambrian basement rocks (Bennett and DePaolo, 1987). This evidence for underlying remnants of Archean(?)-Proterozoic LC-SCML suggests that the ancient LC-SCML was not entirely sheared off in Laramide time.

Sierra Nevada Batholith (*SNB*): Remnants of pre- to syn-Laramide mantle lithosphere that constituted the arc root for the SNB are

present in late Miocene xenolith suites from the central SNB (e.g. Big Creek locality in Fig. 1; Ducea and Saleeby, 1998; Ducea, 2001; Chin et al., 2012). Thermobarometric data from these rocks have been used to construct an ~125 km deep mantle wedge "lithostratigraphy" (Ducea and Saleeby, 1998; Saleeby et al., 2003); with peridotites dominating the base of the section, grading upward into garnet websterite, followed by a ~45 km thick zone of abundant garnet clinopyroxenite (arclogites), which transitions into garnet granulite at ~1.2 GPa conditions (~40 km paleodepth). Geochronologic and trace element and isotopic analysis indicates that the garnet clinopyroxenites are partial melt residues, or deep level cumulates, linked to the overlying SNB (e.g. Ducea and Saleeby, 1998; Ducea, 2001). These garnet clinopyroxenites contain clinopyroxene with diopsidic (not jadeitic) compositions, Type-B garnet, accessory hornblende and orthopyroxene, and less commonly phlogopite and plagioclase. Given their unique geodynamic and petrogenetic significance, instead of "eclogites" (of metamorphosed lower plate origin), these rocks are referred to as "arclogites" (Anderson, 2005)—a term that has been adopted in this paper. The preservation of this ~125 km of arc-root assemblage beneath the central SNB through Miocene time sharply contrasts with the virtual absence of these materials beneath the eastern SCB (Fig. 1).

2.3. Missing SCB lower lithosphere

As to the fate of the missing SCB mantle wedge and arc root (i.e., lower lithosphere), intensified traction associated with the Late Cretaceous flattening of the subducting Farallon plate underneath the Mojave Desert area probably played a key role in "bulldozing" the tectonically eroded LC-SCML ~500 km eastward, to the CPTZ and beyond (Livaccari et al., 1981; Bird, 1988; Saleeby, 2003; Liu et al., 2010; Axen et al., 2018).

The lower crust—upper mantle xenolith assemblages from the Laramide interior can be utilized to reconstruct tectonic displacements in the LC-SCML. The ca. 25 Ma Sullivan Buttes Latite crops out in Chino Valley, Arizona (Fig. 1, 2) and adjacent areas and includes numerous garnet-pyroxene-amphibole rocks, garnet granulites, supracrustal rocks, and subordinate peridotites (e.g. Arculus and Smith, 1979; Esperanca et al., 1998; Smith et al., 1994). The nearby Camp Creek (Esperanca et al., 1988; Erdman et al., 2016) locality (Fig. 1, 2) includes similar xenoliths. These assemblages, possibly the entrained remnants of the displaced lower lithosphere, may be thought of as mantle xenolith "piercing points" that can provide insights into the tectonic erosion and translation of the mantle wedge and arc root. While arclogitic and garnet-websterite xenoliths are present at Camp Creek and Chino Valley, no schist equivalent felsic xenoliths such as those as Cemetery Ridge and Plomosa Mountains are observed at either locations.

If indeed the advancing flat slab bulldozed the SCB LC-SCML eastwards, the remnants of this material, once attached to the base of the SCB, should (1) record isobaric cooling associated with the displacement form hot arc to cooler craton interior under similar lithospheric depths and (2) retain the high-temperature portion of the thermal history of the Mojave Desert (Chapman et al., 2019, 2020), with possible overprints of the late stage (post-Laramide?) thermal evolution of the CPTZ. The Mojave Desert region is chiefly underlain by Jurassic (ca. 160-140 Ma) and Late Cretaceous (90-70 Ma) arc plutonic assemblages with relatively small amounts of Mesozoic to Neoproterozoic sedimentary protoliths, now exposed as metamorphic pendant rocks within batholithic assemblages (Wells and Hoisch, 2008; Barth et al., 2008; Needy et al., 2009; Chapman et al., 2018). If the xenoliths recovered from the CPTZ are indeed consanguineous with the SCB, the xenoliths should chiefly yield Late Cretaceous and Jurassic ages that closely match those of the SCB.

3. Metamorphic petrology

Major element concentrations of minerals (Appendix D1) were determined using a JEOL 6610 LV Scanning Electron Microscope (Energy Dispersive Spectrometry (EDS)) and modal abundance maps of the mineral phases present were obtained using an M4 Tornado Micro X-Ray Fluorescence Spectrometer at Macalester College (Appendix B). For X-ray imaging of Fe, Mg, Ca and Mn distribution in garnet, electron microprobe analyses (EPMA) were conducted with JEOL JXA-8900R electron microprobe at University of Minnesota. Maps were processed to enhance zonation features using *imagesc* (MATLAB).

The studied xenoliths from Chino Valley and Camp Creek, primarily garnet clinopyroxenites (Appendix D2), contain 45-75% modal abundance of almandine garnet and 20-45% diopside clinopyroxene (Appendix B). Rutile (2-3%) occurs as inclusions in garnet and clinopyroxene, and commonly contains variably textured ilmenite exsolution lamellae and patches (Fig. 3c-d). Other mineral phases include apatite, zircon and 5-10% amphibole. The rocks contain Type-B garnet (30-35% pyrope), diopsidic clinopyroxene, and lack phlogopite and plagioclase, except when injected by host latite.

Garnet grains, typically subhedral with kelyphitic rims, range in diameter from ~1-6 mm and show subtle zonation (Appendix C). In samples extensively altered by lava intrusions, some garnets have been completely altered to kelyphite (Fig. 3). The garnet core composition (from sample 16CV2C) is approximately 38 mol% almandine, 35 mol% pyrope, 26 mol% grossular and 1 mol% spessartine ($Alm_{38}Py_{35}Gr_{26}Sp_1$). The rim is slightly enriched in both almandine and grossular components and has a lower pyrope component ($Alm_{39}Py_{31}Gr_{29}Sp_1$). Garnet zonation profiles (Fig. 4) are similar to those observed by Smith et al. (1994) in Chino Valley rocks, and further reveal a monotonic decrease in the Mg# (Mg/(Mg+Fe)) from core to rim.

Matrix clinopyroxene is mainly diopsidic (unzoned) ranging from ~70 to 90 mol% diopside (average ~78 mol%) across different samples. A significant amount of clinopyroxene in the Camp Creek samples has been altered to plagioclase, biotite, K-feldspar, and epidote, presumably during invasion of latite lava (Fig. 3). The rocks also contain up to ~5–10% modal abundance of secondary amphibole (dominantly pargasistic/edenite hornblende) as a late textural replacement of clinopyroxene. In some cases, the amphibole overprint also preserves the clinopyroxene cleavage habit with two distinctive planes intersecting at ~90° angle (Fig. 3e-f).

4. Temperature and pressure estimates

To estimate peak conditions of equilibrium, we constructed a bulk-composition specific equilibrium phase diagram (pseudosection) for the xenoliths and applied major element (garnet-clinopyroxene Fe-Mg exchange) and trace element (Ti-in-zircon and Zr-in-rutile) thermometry. Previous studies estimated temperature and pressure for Chino Valley garnet clinopyroxenite samples at 600-850 °C and 12-28 kbar (Smith et al., 1994; Erdman et al., 2016). The high-pressure constraint (~28 kbar) in these studies have been computed from websterites (i.e. quenched mantle melts instead of arcologitic residues; Chapman et al., 2019), and hence we consider them as upper bound on peak pressures for garnet clinopyroxenites. Another study (Esperanca et al., 1988) estimated similar temperatures for Camp Creek xenoliths at 600-900 °C and constrained the pressure of one plagioclase bearing sample from the same xenolith suite at ~10 kbar. For plagioclase-absent assemblages studied here, this calculated pressure (perhaps a result of late stage equilibration between plagioclase rich melt and the garnet-clinopyroxene phases) provides a low-pressure constraint.

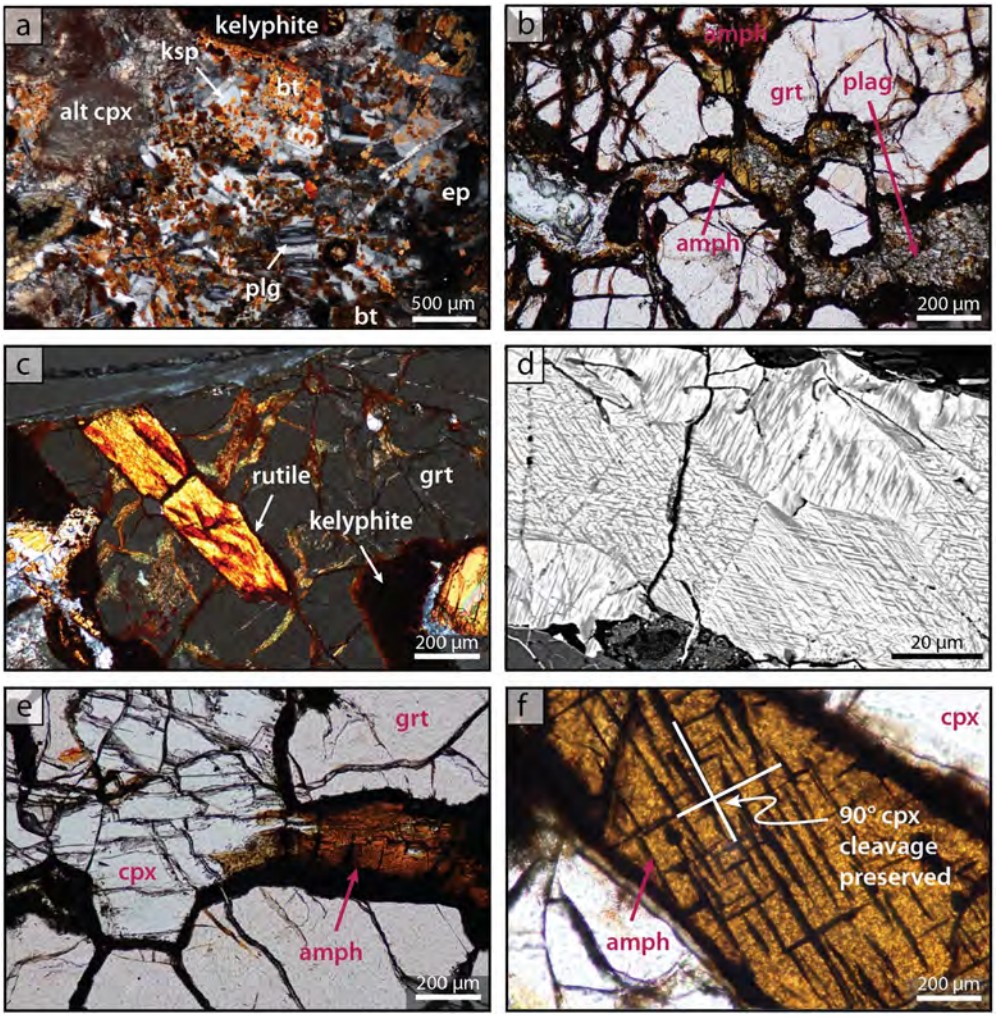

Fig. 3. Xenolith petrography. (a) A pocket of lava consisting of plagioclase, epidote, potassium feldspar and biotite (xpl); 16CC2C. (b) Amphibole altering to plagioclase in lava intruded sample (ppl); (c) Rutile inclusion in a garnet grain (xpl); 16CC2C. (d) ilmenite-rutile exsolution lamellae (white: ilmenite, gray: rutile). (e) Clinopyroxene being replaced by amphibole (ppl); 16CV2FF. (f) Secondary amphibole with preserved clinopyroxene ~90° cleavage (ppl); 16CV2FF. Abbreviations as follows: grt, garnet; cpx, clinopyroxene; amph, amphibole; ksp, potassium feldspar; alt, altered; bt, bitotite; plg, plagioclase; ep, epidote; ppl, plane-polarized light; xpl, cross-polarized light.

4.1. Petrogenetic modeling

Pressure-temperature (PT) field: In the pseudosections constructed for the xenoliths, the assemblage garnet (almandine, grossular, pyrope) + clinopyroxene (diopside) + ilmenite + rutile is stable over a wide range of temperature (>550 °C) and pressure from ~12 kbar to >30 kbar (Fig. 5). Compositional isopleths calculated for almandine (Alm) and pyrope (Py) components of garnet do not intersect at any single point on any phase diagram at values corresponding to those measured. Nevertheless, the general trend of isopleths in the stable P-T field for pyrope mol% decreases and almandine mol% increases (also observed in garnet core to rim zonation profiles; Fig. 4) as the temperature decreases. These observations strongly suggest that garnet growth occurred during cooling. Given the near vertical slope of the isopleths (low sensitivity of the garnet composition with respect to pressure) in the stable PT field, a better constraint cannot be imposed on the peak pressure experienced by the arclogites. Additionally, the grossular content of garnet is not accurately modeled (observed values not present in the stable PT field). These inconsistencies (e.g. no point of intersection of the observed compositional isopleths) are possibly due to inaccurate assumptions about bulk composition, modification (e.g., by diffusion at high temperature) of mineral compositions, or problems with the solution models (the solid solutions are at or near the end-member (maximum range) compositions; e.g., pyrope and grossular in garnet).

Addition of H_2O: Studied xenoliths contain up to ~10% modal abundance of texturally late amphibole replacing clinopyroxene in the assemblage. Secondary amphibole is generally more abundant in highly altered Camp Creek and Chino Valley xenoliths, comprising up to 30% by mode (Fig. 3 e-f). Modeling in *theriak* (Appendix A) for a range of P-T conditions suggests that the xenoliths absorbed at least ~0.2 w.t.% H_2O (2000 ppm) with respect to solid phases present for the bulk compositions specific to these samples (Fig. 6). Modeled amphibole modal abundance and composition (hornblende and pargasite) are consistent with the petrographic observations. The results also show that addition of more than 0.5 w.t.% H_2O with respect to solid phases stabilizes chlorite in the assemblage and given the absence of secondary chlorite in the studied xenoliths, it follows that the rocks experienced moderate late stage hydration (<0.5 w.t.% H_2O with respect to solid phases).

4.2. Major and trace element thermometry

Garnet–clinopyroxene Fe–Mg – Various calibrations for the CPTZ arclogites for garnet-clinopyroxene compositions, over a range of pressure (12 kbar to 28 kbar), yield equilibration temperatures of 700–850 °C (e.g., Nakamura, 2009). These estimates are similar to

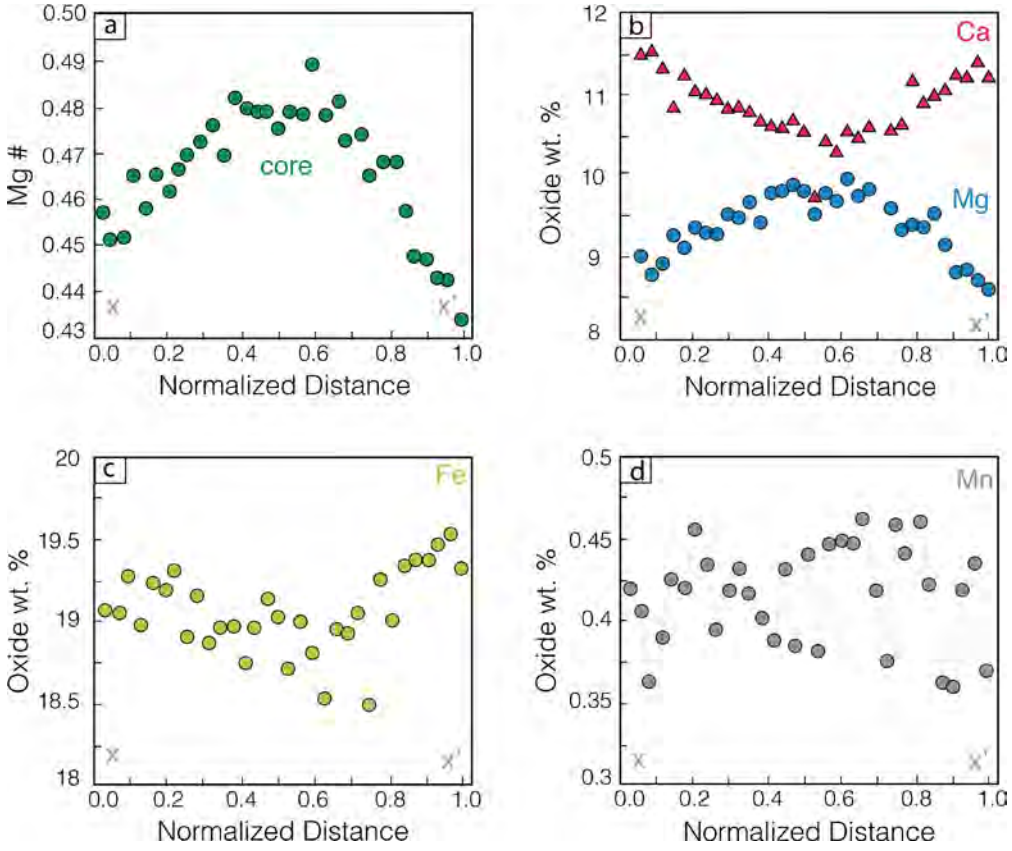

Fig. 4. Growth zonation profiles in arclogite garnet in sample 16CV2C. Location of the zonation profile is shown in Supplementary Fig. 2 (16CV2C Grain 1). (a) Monotonic decrease in Mg# from core to rim (~6 mm). (b) Increase in Ca and decrease in Mg concentration from core to rim. (c) Slight increase in Fe concentration from core to rim. (d) No zonation with respect to Mn in garnet.

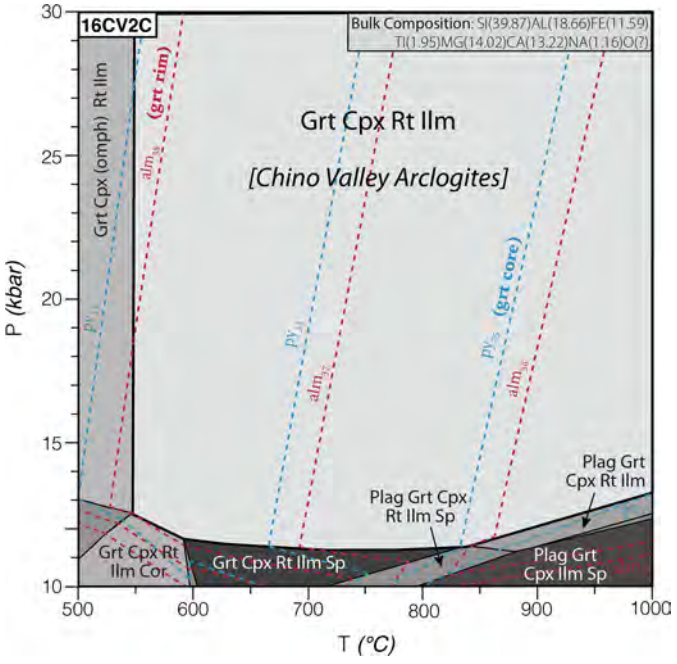

Fig. 5. Psuedosections calculated for 16CV2C using Theriak-Domino. Stable Pressure Temperature (PT) field shown for Chino Valley Arclogites. Garnet almandine (red) and pyrope (blue) isopleths overlays in the stable PT fields, show a general trend of increase in almandine component and decrease in pyrope component with decrease in temperature. Abbreviations as follows: grt, garnet; py, pyrope; alm, almandine; cpx, clinopyroxene; omph, omphacite; do, diopside; rt, rutile; ilm, ilmenite; plag, plagioclase; sph, sphene (titanite); sp, spinel; cor, cordierite. See text for discussion. Method details in Appendix A.

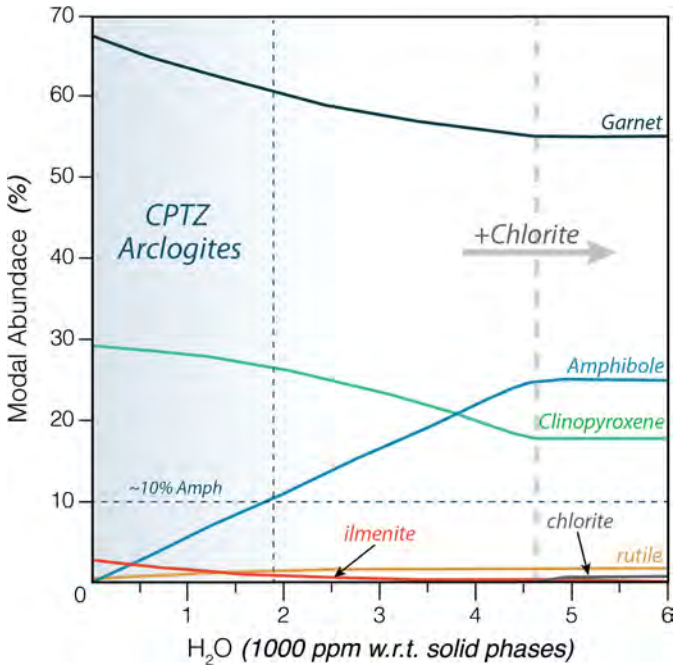

Fig. 6. Influence of H_2O on the arclogite assemblage. Addition of ~2000 ppm (0.2 wt.%) H_2O (w.r.t to solid phases) to the acrologite mineral assemblage results in ~10% modal abundance of amphibole (as observed petrographically). More than ~0.45 wt.% H_2O results in the addition of chlorite phase, which is not observed in the studied arclogites. Modeled in Theriak-Domino.

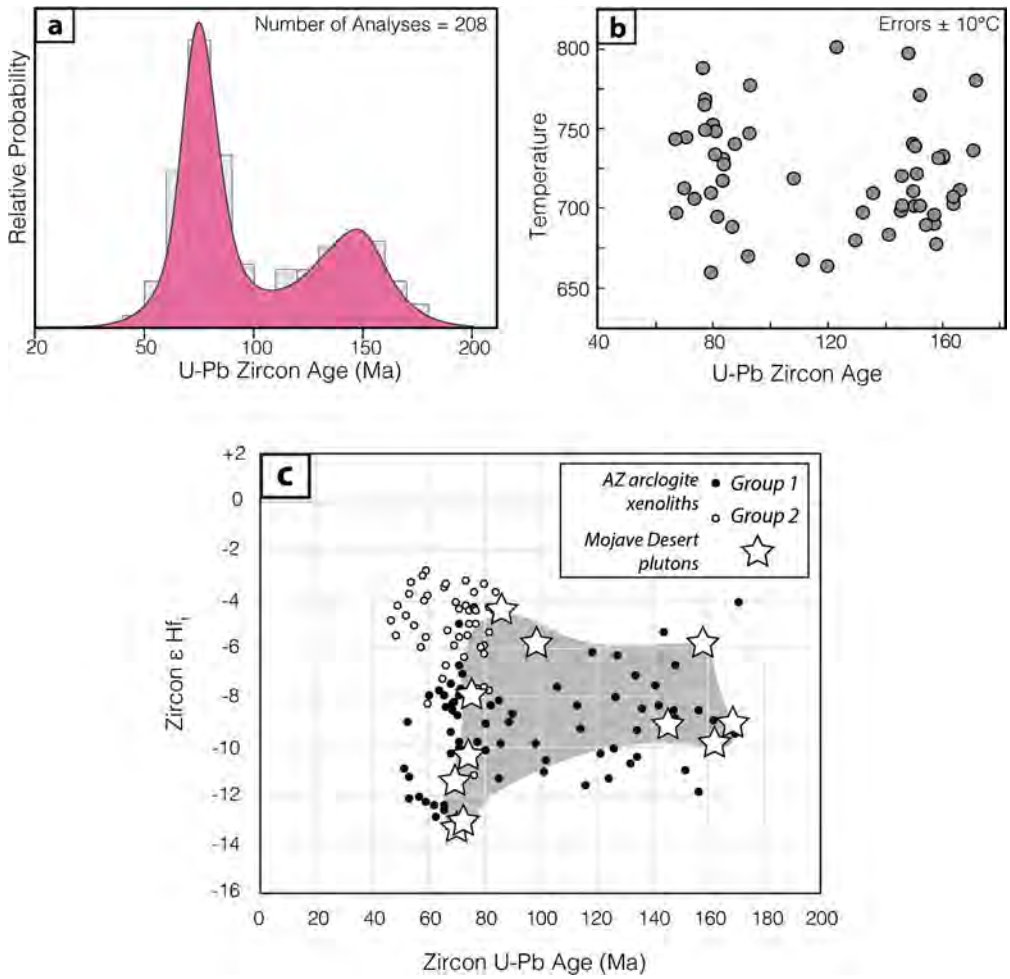

Fig. 7. Zircon U-Pb age distribution and Ti-in-zircon thermometry trend over time. (a) A probability density diagram of U-Pb zircon ages of the samples (data from Chapman et al., 2019). Note two age peaks at ca. 150 Ma and ca. 70 Ma. (b) Ti-in-zircon thermometry (Watson et al., 2006) showing elevated temperatures (>650 °C) from Jurassic through Cenozoic time. See text for discussion. Method details in Appendix A. (c) Zircon Hf evolution diagram comparing Chino Valley and Camp Creek arclogite xenoliths with Mojave Desert plutons (data for the latter from Fisher et al., 2017 and Chapman et al., 2018). Group 1 arclogite are foliated, low-MgO, amphibole-rich, and clinopyroxene-poor; group 2 arclogite are equigranular, high-MgO, amphibole-poor, and clinopyroxene-rich. (Chapman et al., 2019).

those of Smith et al. (1994), Esperanca et al. (1988) and Erdman et al. (2016).

Zr-in-rutile – Rutile grains from Chino Valley samples have a typical composition ranging between ~850-1550 ppm Zr, and those from Camp Creek range from ~650-1350 ppm Zr. One Jurassic sample from Chino Valley sample (sample 16CV2.5F; Sm-Nd age ~153.3 ± 3.1 – *Section 5.2*) has lower Zr concentration (~290-450 ppm) as compared to all other samples. Temperatures calculated using Zr-in-rutile thermometry range from ~730 to 800 °C in Chino Valley samples and ~710 to 785 °C in Camp Creek samples (average ~750 °C).

Ti-in-zircon – Zircon Ti concentrations of the samples range from ~3 to 100 ppm, yielding temperatures from ~650 to 900 °C. In conjunction with existing zircon U-Pb ages (summarized in section 5.1 below; Chapman et al., 2020), thermometry results reveal over ~100 Myr of high temperatures from Jurassic time (average T ~720 °C) through the Late Cretaceous (average T ~750 °C; Fig. 7).

5. Geochronology and zircon trace element analysis

5.1. Zircon U-Pb and trace element analysis

Detailed analysis and discussion of Camp Creek and Chino Valley xenolith U-Pb zircon ages is given in Chapman et al. (2020) and summarized in Fig. 7. With the exception of a small number (<10% of analyzed grains; Chapman et al., 2019, 2020) of latest Cretaceous-early Cenozoic grains, the age distribution of the zircon grains shows two prominent peaks – at ca. 150 Ma (Jurassic) and 75 Ma (Late Cretaceous), suggesting over a ~100 Myr long history of formation/growth.

Zircon REE analyses were done on dated zircon grains by LA-ICP-MS at Rice University, using the same conditions as those described in section 4.2 (Fig. 8). Chondrite-normalized REE patterns show shallow HREE slopes ($Lu_N/Dy_N = 4.53$ to 13.7; average = 7.47). The zircon grains show negative Eu anomalies ($Eu/Eu^* = Eu/\sqrt{Sm_N \cdot Gd_N}$. = 0.14 to 0.82; average = 0.35) that increase (i.e. become more negative) from Jurassic to Late Cretaceous. The zircons also exhibit high positive Ce-anomalies ($Ce/Ce^* = Ce/\sqrt{La_N \cdot Pr_N}$; ranging from ~3.49 to 262.67) with ~70% of the analyzed grains exhibiting $Ce/Ce^* > 50$.

5.2. Garnet Sm-Nd geo-/thermochronology

Two-point Sm-Nd garnet and whole-rock isochrons were calculated from 11 samples (Fig. 9). Analytical methods are in Appendix A. Six samples yield ages and 2σ uncertainties ranging from 33.2 ± 2.4 Ma to 40.1 ± 4.7 Ma and four samples span the range 47.7 ± 1.8 Ma to 59.9 ± 3.1 Ma. The whole rock initial εNd value ranges between −5 and −9 (similar to Esperanca et al., 1998), except for

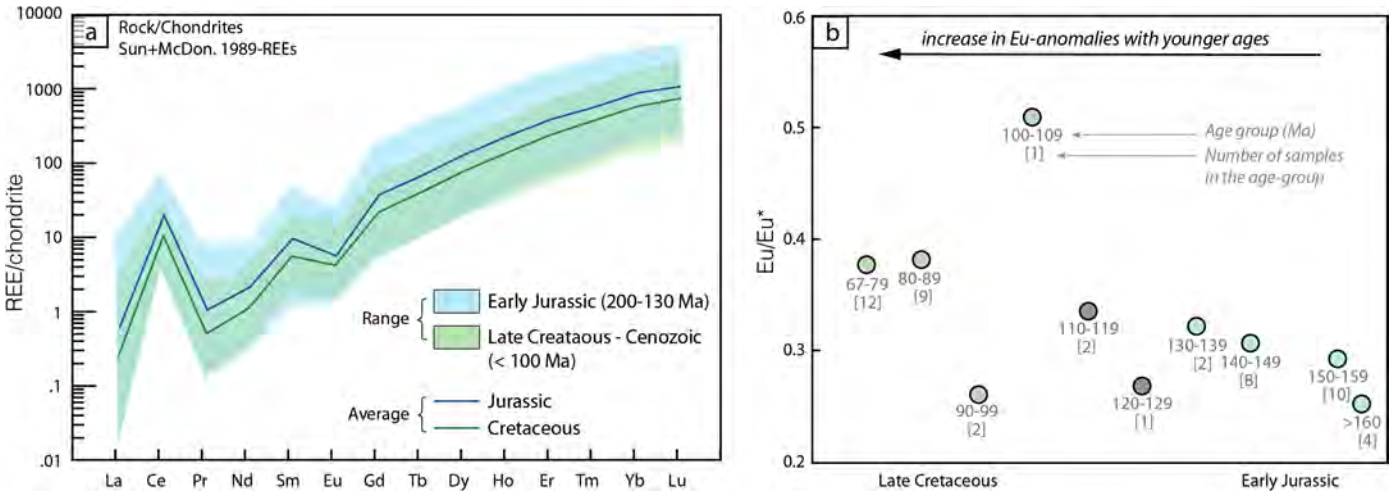

Fig. 8. Chondrite normalized REE plot and Eu-anomalies (Eu/Eu*) for dated zircons. (a) Trends showing the range of REE concentrations and the average in Early Jurassic and Late Cretaceous-Cenozoic periods. Note the positive Ce-anomalies and negative Eu-anomalies. (b) Average Eu anomalies (Eu/Eu*) in the dated zircons showing an increasing trend from Early Jurassic to Late Cretaceous time. See text for discussion; $Eu/Eu^* = Eu/\sqrt{Sm_N \cdot Gd_N}$.

one Chino Valley sample (16CV2.5F), which yields a Jurassic age of 153.3 ± 3.1 Ma and initial whole rock εNd of +8.

6. Discussion

6.1. Evolution of the arclogitic xenoliths

Thermobarometric constraints on the CPTZ xenoliths bracket the peak conditions of equilibration between 12-28 kbar and 650 – 900 °C, which along with the arclogitic composition of the xenoliths (type "B" garnet and diopsidic clinopyroxene) strongly suggests the origin of these rocks as continental arc residues, much like xenoliths recovered from the central SNB. Zircon REE signature, such as HREE depletion, is typically interpreted to indicate the presence of garnet during zircon crystallization, i.e. in eclogite-facies conditions (Rubatto, 2002), also similar to those in which arclogites form. Studied CPTZ arclogites do not contain any plagioclase in the primary mineral assemblage, however the zircons exhibit negative Eu-anomalies. Though the anomalies could be inherited directly from the protolith or source (Rubatto, 2002), the magnitude of the Eu-anomalies increase over time, which in the absence of plagioclase can be explained by Eu being partly reduced (e.g. Tang et al., 2019). Recent studies show that the evolving redox conditions, such as simultaneous oxidation and iron-depletion under reduced conditions (driven by garnet fractionation) in arc magmas, influence the redox-sensitive behavior of Eu resulting in negative Eu anomalies (Tang et al., 2019). Other mechanisms such as initial formation of plagioclase-rich melt and its progressive extraction from the arc-root with plagioclase-free partial melt residue or deep level cumulates left behind (Ducea, 2001; Tang et al., 2019) could have also contributed to the increase in Eu anomalies over time. Interestingly, zircons also exhibit large positive Ce-anomalies (Ce/Ce*); the typical Ce-anomaly of igneous zircon is about ~105 (Vetrin and Skublov, 2015; Rubatto, 2002) and the anomalies calculated for studied zircons are up to 200. Similar to Eu, the behavior of Ce also depends on the redox conditions during zircon crystallization; however, unlike Eu-anomalies, Ce-anomalies increase with the increase in oxygen activity (e.g. Vetrin and Skublov, 2015). The increase in oxidation state of arc magmas is usually attributed to either (1) addition of volatile-rich oxidizing components derived from subducted sediments and oceanic crust to the sub-arc mantle (e.g. Kelley and Cottrell, 2009); and/or (2) oxidation caused by magma differentiation associated with crystallization and chemical interactions with pre-existing crust (e.g., Tang et al., 2019). Both processes, the contamination of the sub-arc mantle with volatiles such as hydrous melts and Ce-rich fluids sourced from the subducting slab and/or from underplated schists and the evolving redox conditions of the arc-magma itself (e.g. Tang et al., 2019), could have contributed to the high positive Ce anomalies observed in the zircons.

Our hypothesis that these arclogites formed as residues to eastern SCB arc magmas and were subsequently bulldozed during the Late Cretaceous flat slab advance, has twofold requirements: first, the thermal evolution of these rock should overlap that of the SCB, with possible post-dispersal thermal overprints and second, the arclogites should record near isobaric cooling associated with the displacement from beneath the hot arc to a colder craton under similar lithospheric depths. The zircon U-Pb ages (Fig. 7) indicate that the lower crust-upper mantle currently underlying the CPTZ formed in two major pulses at ~150 Ma and ~75 Ma, with the bulk of it forming during Late Cretaceous time (Chapman et al., 2020). A detailed analysis of these zircon U-Pb ages in Chapman et al. (2020) clearly shows that the middle Jurassic igneous rocks and early Cenozoic Laramide porphyry copper deposits in SW Arizona with age peaks at ca. 60 and 170 Ma (e.g., Chapman et al., 2018), do not provide as close a match to the CPTZ zircon age distribution. Conversely, the CPTZ xenolith ages more closely overlap with Jurassic plutonism in the SCB associated with subduction of the Farallon Plate beneath North America (Barth et al., 2008; Needy et al., 2009; Chapman et al., 2018) and Late Cretaceous arc magmatism prior to and during shallowing of the angle of the down-going plate (Wells and Hoisch, 2008; Needy et al., 2009; Chapman et al., 2018).

The Jurassic garnet-whole rock Sm-Nd age of 153.3 ± 3.1 Ma of Chino Valley sample 16CV2.5F is interpreted to be a quenched peridotite-derived melt in the mantle. An initial εNd of +8, strongly suggests derivation from a recently depleted mantle, likely associated with Jurassic magmatism in the Mojave Desert region. Alternatively, the sample could also have been derived from the oceanic Farallon crust, however, sample 16CV2.5F (and other similar samples from Chino Valley and Camp Creek) contains orthopyrexene, i.e. it is a websterite. The sample also contains type B garnet (Smith et al., 1994) and diopsidic clinopyroxene which is more compatible with a mantle derived melt (for Farallon crust derived sample, we would expect omphacitic clinopyroxene instead). The zircons extracted from Camp Creek garnet-clinopyroxenite xenoliths also yield low negative εHf values (−3 to −13), time-corrected to corresponding U-Pb ages (Fig. 7c). A significant Pre-

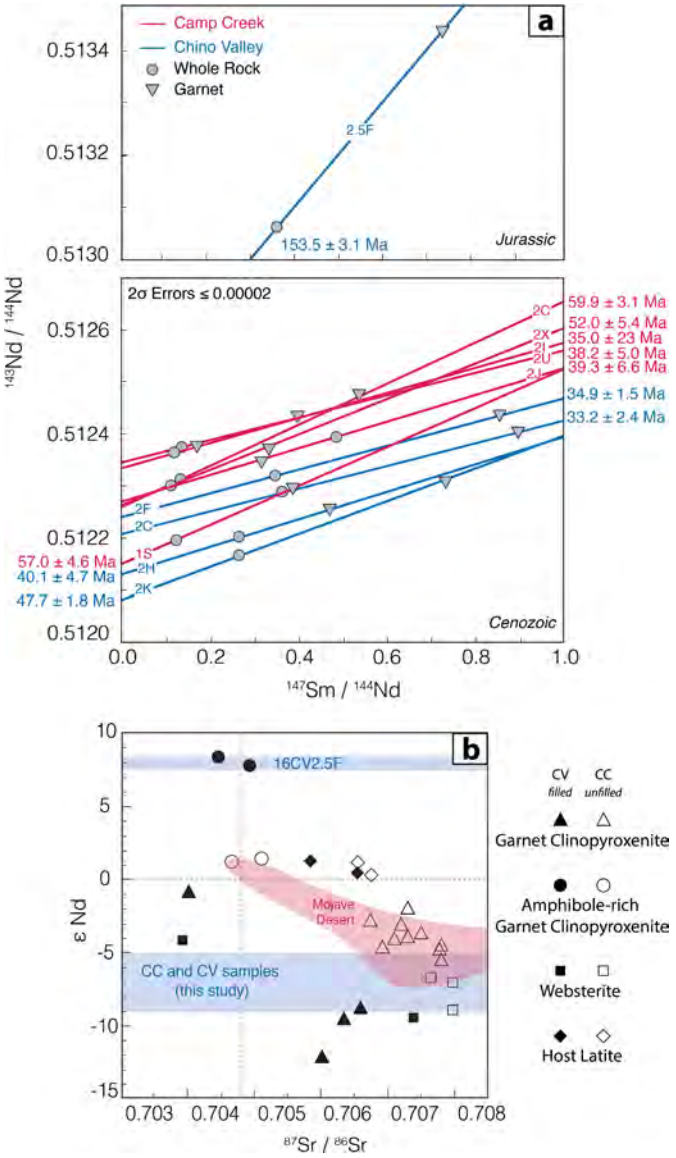

Fig. 9. (a) **Sm-Nd garnet-whole rock geochronology.** One Chino Valley sample 16CV2.5F records a Jurassic age. Remaining samples yield Late Cretaceous–Early Cenozoic ages, suggesting partial re-equilibration of the samples with host latite. (Chapman et al., 2019). (b) **Sr and Nd isotopic compositions** for Chino Valley (*CV, filled*) and Camp Creek (*CC, unfilled*) xenoliths compared to plutonic rocks of the Mojave Desert (shaded pink). Data from Esperanca et al. (1998), Smith et al. (1994), Miller et al. (1996), and this study (shaded blue, note Sr isotopic data are not available for this study). Intersecting axes are "bulk earth" values. Epsilon values and Sr ratios are initial values for xenoliths; values from Mojave Desert plutons are age-corrected for 90 Ma.

cambrian lower lithosphere component is required to explain low negative εNd and εHf values from these nodules. Zircon εHf values from plutons of the Mojave Desert (Fisher et al., 2017; Chapman et al., 2018) overlap those of Arizona arclogite xenoliths, further corroborating the assertion that Arizona arclogites represent mafic restites/cumulates genetically related to the SCB (Chapman et al., 2019).

In addition to the high-temperature portion of the thermal history of the Mojave Desert Region, these xenoliths also contain evidence for possible overprints of the late stage (syn/post-Laramide) thermal evolution of CPTZ. Garnet-whole rock Sm-Nd ages range from ~33 to 60 Ma and yield low negative initial εNd values (−5 to −9), precluding derivation from oceanic crust or young depleted mantle and instead requiring extraction from Precambrian lower crust (and/or mantle material). The closure temperature, calculated at ~725 °C for a 1 mm garnet, is similar to the peak estimates from garnet-clinopyroxene thermometry (~700–850 °C). Additionally, titanite derived from multiple samples of Chino Valley garnet clinopyroxenite yields an age of ca. 57 Ma that overlaps garnet-whole rock ages at the 1σ level (Erdman et al., 2016). Considering that arclogitic nodules equilibrated at temperatures overlapping garnet Sm-Nd and titanite U-Pb closure temperatures, the observed Cenozoic spread in garnet and titanite ages suggests that these rocks were at or above Sm-Nd garnet closure temperatures for a protracted interval of time (Chapman et al., 2020). The elevated temperatures in the region associated with Eocene to Miocene westward sweep of magmatism, including the ca. 25 Ma arclogite xenolith-hosting latite, that accompanied rollback and tearing of the Farallon slab (e.g. Coney and Reynolds, 1977), may also be responsible for partial re-equilibration of the Sm-Nd systematics in the samples relative to the Jurassic Chino Valley sample 16CV2.5F (Fig. 9). These data, along with Ti-in-zircon thermometry point to long-term (10s of Myr) residence within the lower lithosphere at high temperatures (>700 °C) and/or incomplete re-equilibration with ca. 25 Ma host latite.

The Jurassic to Late Cretaceous-Early Cenozoic thermal history of studied xenoliths, in conjunction with the thermobarometric data, indicates the growth and/or equilibration of xenoliths over ~100 Myr at elevated temperatures (>700 °C) and pressures (>12 kbar). The pressure range of 12-28 kbar (45-100 km depth assuming a 2800 kg/m^3 overburden density; Smith et al., 1994; Esperanca et al., 1988; Erdman et al., 2016) associated with the formation of these rocks, is similar to that expected for the sub-SNB garnet-clinopyroxenite suite (e.g., Ducea and Saleeby, 1998; Saleeby et al., 2003; Chin et al., 2012). Pseudosections showing nearly isothermal almandine and pyrope garnet isopleths in the field of interest further shed light on the general PT evolution of the rocks (Fig. 5). The garnet rims are characterized by increasing almandine and decreasing pyrope component, indicating that conditions of decreasing temperatures during late stages of garnet growth in these bulk compositions (Figs. 6 and 7, Appendix C). The garnet grains also exhibit growth related zonation associated with a monotonic decrease in the Mg# from core to the rim, recording garnet growth during cooling conditions (~300 °C) (Spear, 1993). Cenozoic Sm-Nd garnet and U-Pb titanite ages (Esperanca et al., 1988; Smith et al., 1994; Erdman et al., 2016) indicate that the arclogites remained hot (>700 °C) through Late Cretaceous until Miocene. Thus, it is likely that growth zonation captures the cooling of the LC-SCML in its latest-stages of formation, as it migrated eastwards from the hot continental arc (SCB) to colder interior craton in Late Cretaceous. Alternatively, it could be argued that isobaric cooling occurred following construction of an arclogitic root to Laramide porphyry copper deposits. However, the geochronologic relations provided herein render this possibility unlikely.

Late stage hydration event: Xenolith petrography reveals partial replacement of clinopyroxene by amphibole (Fig. 3e, f), raising the possibility that these rocks experienced a late-stage hydration event. Thermodynamic modeling results show that for the bulk composition of studied arclogites, addition of at least 0.2 w.t.% H_2O (with respect to solid phases present in the samples) is required to obtain the amphibole modal abundance and composition (hornblende and pargasite) that is consistent with petrographic observations. Several studies suggest that the flattening of the Farallon slab introduced water into the North American lithospheric mantle during Late Cretaceous time (e.g. Lee, 2005 and references within). The hydration of the LC-SCML driven by dewatering of the subducting Farallon plate could explain the presence of secondary amphibole. Dehydration of subducted sediments (either directly from the subducting slab or from the underplated trench-derived mate-

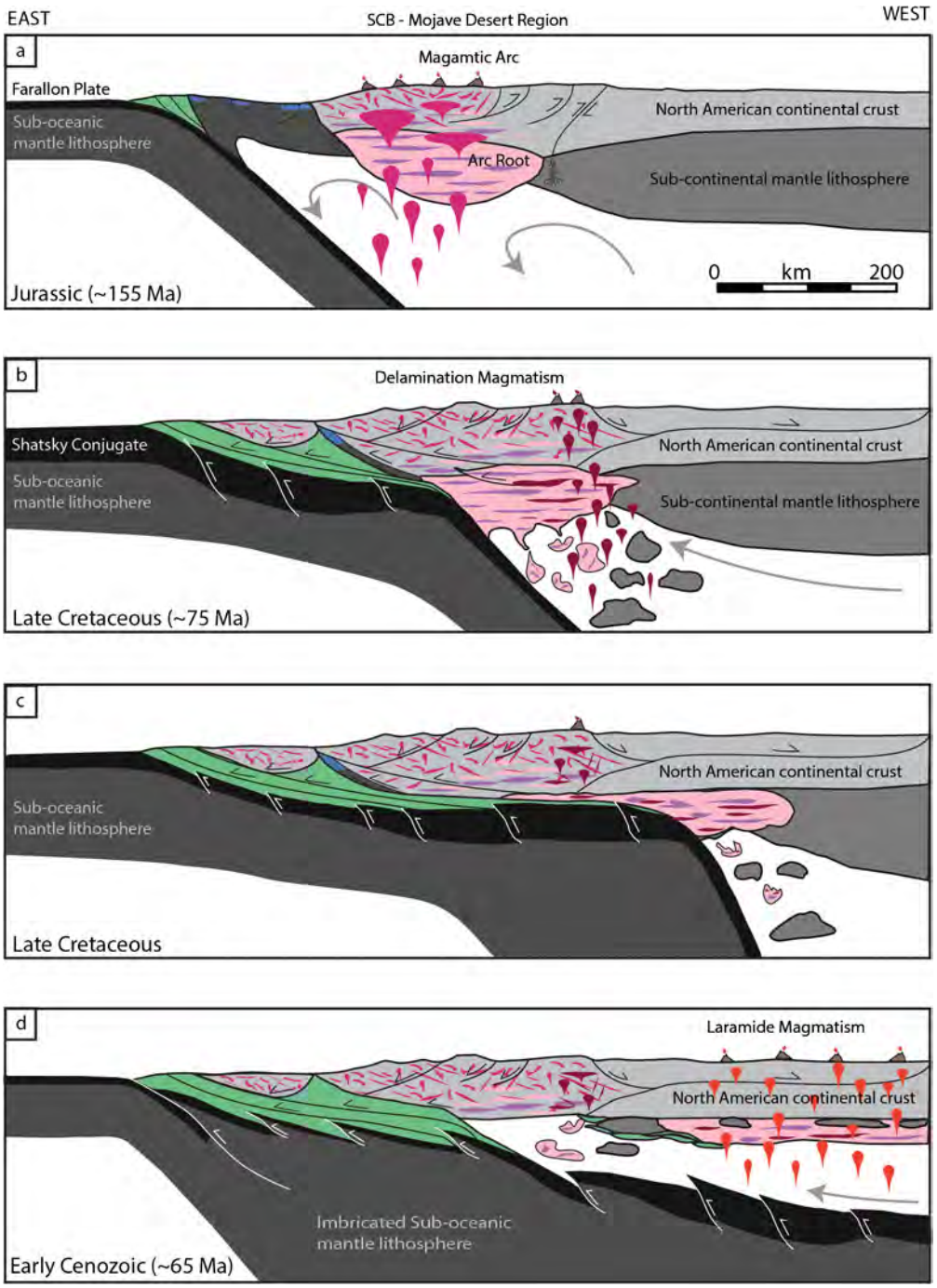

Fig. 10. Tectonic cartoons illustrating tectonic evolution of the LC-SCML underlying the Mojave Desert region (Jurassic to Early Cenozoic). Key: green, trench sediments; pink, maroon and orange drops, magmatism; arrows; inferred mantle-asthenosphere flow/convection. See text for discussion. Modified from Wells and Hoisch (2008) and Chapman et al. (2020).

rial dislodged with the sub-SCB arc root, Fig. 10), could have also introduced Ce-rich fluids into the LC-SCML contributing to the high Ce-anomalies observed in CPTZ arclogite zircons. Alternatively, the amphibole formation may be related to magmatism and the main formation stage of the arclogites themselves, which is often seen in other arclogitic xenoliths from the SNB (Ducea and Saleeby, 1998). However, this seems unlikely given the petrographic evidence that amphibole in CPTZ arclogites is present as late textural replacement of clinopyroxene (Fig. 3e-f). It could also be argued that hydration of the studied xenoliths was accomplished by interactions with high-H_2O latite and did not require an earlier phase of hydration. We consider this unlikely given that alteration of arclogitic xenoliths by host lavas occurs at a fine scale (e.g., development of sub-µm oxide-silicate intergrowths on garnet/clinopyroxene), due to the very limited amounts of time xenoliths are exposed to the lavas (on the order of days; Heger, 2013 and reference within) and does not involve the much larger scale (100s of µm) growth of secondary amphibole (Fig. 3e, f). Furthermore, the fluid-fluxed growth of amphibole at the expense of clinopyroxene in arclogite should also have been accompanied by the addition of aqueous silica (e.g., Manning, 1997), which does not appear to be the case in studied arclogite samples. We suggest that any silica migrating upward from the Farallon slab and/or underplated schist was buffered by talc and serpentine within a few km of the subduction

megathrust (Manning, 1997), leaving overriding arclogite hydrated yet relatively unsilicified.

6.2. Tectonic bulldozing of the LC-SCML

The geo-thermochronologic and geochemical relations together indicate that origin of CPTZ xenoliths as continental arc-residues with overlapping thermal history with the SNB-Mojave-desert region. Thermobarometric data consistent with the hypothesized displacement of these rocks, lead us to assert that these arclogitic xenoliths are not native to central Arizona and instead represent lower crustal-upper mantle materials displaced eastward from beneath the SCB and reaffixed beneath the CPTZ region. We now focus on the petrologic and tectonic evolution of CPTZ arclogites (Fig. 10).

Xenoliths of the CPTZ began forming in the Late Jurassic (Fig. 10a) as deep level cumulates/partial melt residues (45-100 km depth) to continental arc magmas in the Mojave Desert Region. During Late Cretaceous, the Farallon slab outboard of the Mojave Desert Region evolved into a shallow-flat geometry (e.g. Livaccari et al., 1981; Liu et al., 2010). As a result, upper-lower plate traction and lateral stresses intensified, destabilizing the LC-SCML under the Mojave Desert region, facilitating upwelling of asthenosphere and igniting a pulse of Late Cretaceous arc activity (e.g. Wells and Hoisch, 2008). It was during this period of increased arc magmatism that the sub-SCB root experienced another pulse of growth at ca. 80-70 Ma as recorded by the zircon U-Pb ages (Wells and Hoisch, 2008; Needy et al., 2009; Chapman et al., 2018, 2020). As the flat slab continued to advance, the destabilized arc-root dislodged from the SCB above and underplated schists were tectonically bulldozed along the tip of the shallow slab segment from its origin to at least ~500 km further inboard (Fig. 10c) to the CPTZ (Chapman et al., 2019, 2020). The arclogite experienced cooling as it was displaced from underneath the hot arc to under colder craton as recorded by garnet zonation profiles; however the displaced material continued to remain hot (>700 °C) for 10s of Myr following its dispersal, until eruption in late Oligocene-Miocene, as indicated by Cenozoic Sm-Nd garnet and U-Pb titanite ages (Esperanca et al., 1988; Smith et al., 1994; Erdman et al., 2016; this study). With continued plate convergence and advance of flat slab further inboard with a dislodged LC-SCML at it leading edge, the foreland crust thickened significantly, forming a high-elevation plateau (DeCelles, 2004; Copeland et al., 2017). Magmatism also swept inboard at this time, forming ca. 75-55 Ma granitic stocks and large calderas and associated copper mineralization in the transition zone (e.g., Chapman et al., 2018). As suggested in Chapman et al. (2019, 2020), crustal thickening-related radiogenic heating and increased magmatic activity in the Colorado Plateau region likely precipitated Latest Cretaceous-early Cenozoic zircon growth in dislodged arclogite and also partially re-equilibrated the garnet Sm-Nd system as well.

Recent geodynamic studies (Axen et al., 2018) modeling the effects of evolving morphology of the subducting Farallon plate on the LC-SCML underneath the S.W. Cordillera are consistent with the interpretations above. Following the start of flat-slab subduction, the thermomechanical models predict underplating of continental crust with trench-derived sediments (such as the underplated San Emigdio schists in the Mojave region; Fig. 10c, d) and also the shearing of ~20-50 km of LC-SCML as a result of the shallowing angle of subduction (Jacobson et al., 1988; Barth et al., 2008; Grove et al., 2003; Saleeby, 2003; Ducea and Chapman, 2018; Chapman et al., 2012). In these models the flat slab scrapes off or tectonically erodes the LC-SCML, which then migrates ahead of the advancing slab, perhaps as far as SW Colorado. In the models, the displaced LC-SCML resists sinking with the slab, instead remains intact underneath the continental crust even after the slab roll-back, much like our hypothesized displacement of the sub-SCB arclogite and trench-derived material and their re-affixation beneath the CPTZ and further inboard (Fig. 10c, d).

6.3. Implications for Cenozoic tectonism in SW U.S.

Strength of the Colorado Plateau relative to adjacent provinces: The tectonic stability of the Colorado Plateau through the Laramide contractile and Cenozoic extensional deformation in SW U.S. remains a longstanding enigma in Cordilleran tectonics (e.g., Morgan and Swanberg, 1985). A commonly cited reason is the strength offered by the cold and thick lithosphere of the Colorado Plateau (e.g. Lee et al., 2001). However, various seismic and isotopic studies independently indicate that the lithosphere of the Colorado Plateau mantle lithosphere was neither stronger nor thicker than that of the adjacent Basin and Range, prior to Mesozoic and later deformation events (e.g., Bird, 1988; Livaccari and Perry, 1993). Instead, Bashir et al. (2011) suggests that a mafic layer, presumably the displaced arclogite material, underlies most of the Colorado Plateau at ~30-40 km depth. This mechanically strong mafic keel might have provided additional support for the Colorado Plateau to remain stable relative to adjacent geologic provinces (Bashir et al., 2011). Late Cretaceous displacement and attachment of arclogite to the base of the Colorado Plateau in Late Cretaceous time are compatible with this view. We speculate that the addition of LC-SCML material in the region had an "armoring/hardening" effect, further contributing to the stability of the region and producing the tectonomorphically distinct plateau, until (as discussed below) these dense materials began to founder in middle Cenozoic time (e.g. Levander et al., 2011; Erdman et al., 2016).

Post-Laramide extensional regime: The Colorado Plateau and adjacent transition zone, the inferred location of displaced arclogite, has undergone significant post-Laramide extensional tectonism. Re-affixation of a foreign LC-SCML from a region of high arc magmatism (SCB) to underneath the Colorado Plateau region, might have preconditioned the region to Oligocene-Miocene regional extension, formation of Cordilleran core complexes and post-Miocene delamination. Vertically dipping seismically fast features and the presence of a "double Moho" within the CPTZ (Levander et al., 2011; Erdman et al., 2016) and the abundance of spinel peridotite xenoliths (instead of arclogites) in Miocene and younger volcanic host rocks, suggests that these dense materials began to founder and be replaced by upwelling asthenosphere in middle Cenozoic time, at ~12 Ma and perhaps as early as 25 Ma, e.g. (Levander et al., 2011; Erdman et al., 2016). The timing of arclogite delamination overlaps that of the onset of extension and development of the southern belt (i.e., California, Arizona, and Sonora) of Cordilleran metamorphic core complexes (e.g., Dickinson, 2009) suggesting a possible genetic relationship. The post-Laramide roll-back of the Farallon slab and associated influx of asthenosphere destabilized and led to the foundering of the foreign mafic keel of the Colorado Plateau (rather than native cratonic lithosphere e.g., Levander et al., 2011), leaving the overlying crust exposed to asthenospheric upwellings. Ensuing flow in the weakened lower crust facilitated the localized surface extension and further crustal thinning in the upper crust, ultimately resulting in the prevalence of an extensional regime; i.e. the formation of southern belt of Cordilleran metamorphic core complexes. Meanwhile, the interior of the Colorado Plateau appears to be underlain by a thick lithospheric mantle, composed of cratonic material and underlying mafic (arclogitic?) layer which, we speculate, continues to protect the crust from deep convecting mantle, contributing to the tectonic stability of the plateau.

7. Conclusion

We have integrated new and existing (e.g. Esperanca et al., 1988; Smith et al., 1994; Erdman et al., 2016) petrogenetic and geo-thermochronologic studies of LC-SCML xenoliths to understand the tectonic evolution of the SW Cordillera lower lithosphere, specifically the fate of missing sub-SCB materials. Arclogitc compositions of these rocks at high PT conditions of equilibration (600-900 °C, 12-28 kbar) and a bimodal U-Pb zircon age distribution overlapping that of the Mojave Desert region strongly implies the formation of these rocks as a continental arc root to the SCB. Titanite ages and Cenozoic Sm-Nd whole rock-garnet ages point toward post-displacement thermal overprints, perhaps a result of long-term (10s of Myr) residence within the lower lithosphere and/or incomplete re-equilibration with ca. 25 Ma host latite in CPTZ region. Zircon REE abundances suggest concurrent growth of garnet and zircon, while garnet zonation patterns record growth during cooling, likely related to the >500 km displacement from the hot SCB to colder CPTZ. Negative Eu-anomalies and positive Ce-anomalies observed in the zircons could be a product of evolving redox conditions in the arc system itself (e.g. Tang et al., 2019) and/or contamination of the arc magmas by volatiles from the subducted oceanic crust and/or underplated schists.

The petrologic and tectonic relations presented herein lead us to assert that arclogitic xenoliths are not native to central Arizona and instead represent LC-SCML fragments displaced eastward from beneath the SCB and reaffixed beneath the CPTZ (Axen et al., 2018; Chapman et al., 2019, 2020). This displaced LC-SCML fragment might also have provided the ballast necessary for the strength of the Colorado Plateau relative to adjacent geologic provinces, providing an intriguing explanation for the tectonic stability of the region through Late Cretaceous and Cenozoic deformation events (e.g., Morgan and Swanberg, 1985; Bashir et al., 2011; Erdman et al., 2016). Destabilization of this foreign mafic keel under the Colorado Plateau ensuing the Farallon slab-roll back, may have also preconditioned the region to Cenozoic tectonism e.g. active delamination, high-magnitude extension and formation of metamorphic core complexes (e.g., Levander et al., 2011; Erdman et al., 2016; Chapman et al., 2020).

Declaration of competing interest

The authors declare that they have no known competing financial interests or personal relationships that could have appeared to influence the work reported in this paper.

Acknowledgements

This effort benefited from assistance by D. Abboud, B. Hunter and J. Thole at Macalester College; A. von der Handt at University of Minnesota; and discussions with S. Esperança and D. Smith. This work was supported by NSF grants EAR-1524768 (to ADC) and EAR-1725002 (to MND) and Romanian UEFISCDI project PN-III-P4-ID-PCCF-2016-0014 (to MND). We appreciate constructive reviews by Richard Carlson and Marty Grove.

Appendix. Supplementary material

Supplementary material related to this article can be found online at https://doi.org/10.1016/j.epsl.2020.116447.

References

Anderson, D.L., 2005. Large igneous provinces, delamination, and fertile mantle. Elements 1, 271–275.

Arculus, R.J., Smith, D., 1979. Eclogite, pyroxenite, and amphibolite inclusions in the Sullivan Buttes latite, Chino Valley, Yavapai County, Arizona. In: The Mantle Sample: Inclusions in Kimberlites and Other Volcanics. American Geophysical Union, pp. 309–317.

Axen, G.J., van Wijk, J.W., Currie, C.A., 2018. Basal continental mantle lithosphere displaced by flat-slab subduction. Nat. Geosci. https://doi.org/10.1038/s41561-018-0263-9.

Barth, A.P., Wooden, J.L., Howard, K.A., Richards, J.L., 2008. Late Jurassic plutonism in the southwest U.S. Cordillera. In: Wright, J.E., Shervais, J.W. (Eds.), Ophiolites, arcs and batholiths: a tribute to Cliff Hopson. In: Geological Society of America Special Paper, vol. 438, pp. 379–396.

Bashir, L., Gao, S.S., Liu, K.H., Mickus, K., 2011. Crustal structure and evolution beneath the Colorado Plateau and the southern Basin and Range Province: results from receiver function and gravity studies. Geochem. Geophys. Geosyst. 12, Q06008. https://doi.org/10.1029/2011GC003563.

Bennett, V.C., DePaolo, D.J., 1987. Proterozoic crustal history of the western United-States as determined by neodymium isotopic mapping. Geol. Soc. Am. Bull. 99, 674–685.

Bird, P., 1988. Formation of the Rocky Mountains, western United States: a continuum computer model. Science 239, 1501–1507.

Chapman, A.D., Saleeby, J., Wood, D.J., Piasecki, A., Kidder, S., Ducea, M., Farley, K., 2012. Late Cretaceous gravitational collapse of the southern Sierra Nevada batholith, California. Geosphere 8, 314–341. https://doi.org/10.1130/GES00740.1.

Chapman, A.D., 2017. The Pelona–Orocopia–Rand and related schists of southern California: a review of the best-known archive of shallow subduction on the planet. Int. Geol. Rev. 59 (5–6), 664–701. https://doi.org/10.1080/00206814.2016.1230836.

Chapman, A.D., Riggs, N., Ducea, M.N., Saleeby, J.B., Rautela, O., Shields, J., 2019. Tectonic development of the Colorado Plateau Transition Zone, central Arizona: insights from lower lithosphere xenoliths and volcanic host rocks. In: Pearthree, P.A. (Ed.), Geologic Excursions in Southwestern North America. In: Geological Society of America Field Guide, vol. 55, pp. 209–235.

Chapman, A.D., Rautela, O., Shields, J.E., Ducea, M.N., Saleeby, J.B., 2020. Fate of continental lower crust and upper mantle during shallow-angle subduction: the Laramide example. GSA Today 30. https://doi.org/10.1130/GSATG412A.1.

Chapman, J.B., Dafov, M.N., Gehrels, G., Ducea, M.N., Valley, J.W., Ishida, A., 2018. Lithospheric architecture and tectonic evolution of the southwestern U.S. Cordillera: constraints from zircon Hf and O isotopic data. Geol. Soc. Am. Bull. https://doi.org/10.1130/B31937.1.

Cheadle, M.J., Czuchra, B.L., Byrne, T., Ando, C.J., Oliver, J.E., Brown, L.D., Kaufman, S., Malin, P.E., Phinney, R.A., 1986. The deep crustal structure of the Mojave Desert, California, from COCORP seismic reflection data. Tectonics 5, 293–320. https://doi.org/10.1029/TC005i002p00293.

Chin, E., Lee, C.T., Luffi, P., 2012. Deep lithospheric thickening and refertilization beneath continental arcs: case study of the P, T and compositional evolution of peridotite xenoliths from the Siera Nevada, California. J. Petrol. 53, 477–511.

Coney, P.J., Reynolds, S.J., 1977. Flattening of the Farallon slab. Nature 270, 403–406.

Copeland, P., Currie, C.A., Lawton, T.F., Murphy, M.A., 2017. Location, location, location: the variable life span of the Laramide orogeny. Geology 45, 223–226. https://doi.org/10.1130/G38810.1.

DeCelles, P.G., 2004. Late Jurassic to Eocene evolution of the Cordilleran thrust belt and foreland basin system, western US. Am. J. Sci. 304 (2), 105–168. https://doi.org/10.2475/ajs.304.2.105.

Dickinson, W.R., 2009. Anatomy and global context of the North American Cordillera. In: Kay, S.M., Ramos, V.A., Dickinson, W.R. (Eds.), Backbone of the Americas: Shallow Subduction, Plateau Uplift, and Ridge and Terrane Collision. In: Geological Society of America Memoirs, vol. 204, pp. 1–29.

Ducea, M.N., Chapman, A.D., 2018. Sub-magmatic arc underplating by trench and forearc materials in shallow subduction systems, a geologic perspective and implications. Earth-Sci. Rev. 185, 763–779. https://doi.org/10.1016/j.earscirev.2018.08.001.

Ducea, M.N., 2001. The California Arc: thick granitic batholiths, eclogitic residues, lithospheric-scale thrusting, and magmatic flare-ups. GSA Today 11, 4–10.

Ducea, M.N., Saleeby, J.B., 1998. The age and origin of a thick mafic-ultramafic keel from beneath the Sierra Nevada batholith. Contrib. Mineral. Petrol. 133, 169–185.

Erdman, M.E., Lee, C.-T.A., Levander, A., Jiang, H., 2016. Role of arc magmatism and lower crustal foundering in controlling elevation history of the Nevadaplano and Colorado Plateau: a case study of pyroxenitic lower crust from central Arizona, USA. Earth Planet. Sci. Lett. 439, 48–57.

Esperanca, S., Carlson, R.W., Shirey, S.B., 1988. Lower crustal evolution under central Arizona: Sr, Nd, and Pb isotopic and geochemical evidence from mafic xenoliths of Camp Creek. Earth Planet. Sci. Lett. 90, 26–40.

Esperanca, S., Walker, R.J., Luhr, J.F., Aranda-Gomez, J.J., 1998. Provinciality in the Mexican lithospheric mantle: Re-Os isotopic evidence from mantle peridotite xenoliths. Eos Trans. AGU 7945 (Fall Meet. Suppl.), F966.

Fisher, C.M., Hanchar, J.M., Miller, C.F., Phillips, S., Vervoort, J.D., Whitehouse, M.J., 2017. Combining Nd isotopes in monazite and Hf isotopes in zircon to understand complex open-system processes in granitic magmas. Geology 45, 267–270. https://doi.org/10.1130/G38458.1.

Grove, M., Jacobson, C.E., Barth, A.P., Vucic, A., 2003. Temporal and spatial trends of Late Cretaceous-early Tertiary underplating Pelona and related schist beneath Southern California and southwestern Arizona. Spec. Pap., Geol. Assoc. Can. 374, 381–406.

Haxel, G., Jacobsen, C., Wittke, J.H., 2014. Mantle peridotite in newly discovered far-inland subduction complex. Int. Geol. Rev. https://doi.org/10.1080/00206814.2014.928916.

Heger, S.E., 2013. Thermobarometry and Geochronology of Mid-Tertiary Alkalic Lavas, Chino Valley, Arizona: Relation to Metamorphic Core Complexes. M.S. thesis. Flagstaff, Northern Arizona University. 163 p.

Jacobson, C.E., Dawson, M.R., Postlethwaite, C.E., 1988. Structure, metamorphism, and tectonic significance of the Pelona, Orocopia, and Rand schists, Southern California. In: Ernst, W.G. (Ed.), Metamorphism and Crustal Evolution of the Western United States, Rubey Volume. Prentice-Hall, Englewood Cliffs, New Jersey, pp. 976–997.

Kelley, K.A., Cottrell, E., 2009. Water and the oxidation state of subduction zone magmas. Science 325, 605–607.

Lee, C.T., Yin, Q.Z., Rudnick, R.L., Jacobsen, S.B., 2001. Preservation of ancient and fertile lithospheric mantle beneath the southwestern United States. Nature 411, 69–73.

Lee, C.T., 2005. Trace element evidence for hydrous metasomatism at the base of the North American lithosphere and possible association with Laramide low-angle subduction. J. Geol. 113 (6), 673–685.

Levander, A., Schmandt, B., Miller , M.S., Liu, K., Karlstrom, K.E., Crow, R.S., Lee, C.-T.A., Humphreys, E.D., 2011. Ongoing Colorado Plateau uplift by delamination-style convective lithospheric downwelling. Nature 472, 461–465. https://doi.org/10.1038/nature10001.

Liu, L., Gurnis, M., Seton, M., Saleeby, J., Mueller, R.D., Jackson, J.M., 2010. Predictions of oceanic plateau subduction beneath North America from plate reconstructions and inverse convection models. Nat. Geosci. https://doi.org/10.1038/NGEO829.

Livaccari, R.F., Burke, K., Sengor, A.M.C., 1981. Was the Laramide orogeny related to subduction of an oceanic plateau? Nature 289, 276–278.

Livaccari, R.F., Perry, F.V., 1993. Isotopic evidence for preservation of Cordilleran lithospheric mantle during the Sevier-Laramide Orogeny, western United-States. Geology 21, 719–722.

Luffi, P., Saleeby, J., Lee, C.T.A., Ducea, M., 2009. Lithospheric mantle duplex beneath the central Mojave Desert revealed by xenoliths from Dish Hill, California. J. Geophys. Res. https://doi.org/10.1029/2008JB005906.

Manning, C.E., 1997. Coupled reaction and flow in subduction zones: silica metasomatism in mantle wedge. In: Jamtveit, B., Yardley, B.W.D. (Eds.), Fluid Flow and Transport in Rocks, Mechanisms and Effects, pp. 139–147.

Miller, J.S., Glazner, A.F., Crowe, D.E., 1996. Muscovite–garnet granites in the Mojave Desert, relation to crustal structure of the Cretaceous arc. Geology 24 (4), 335–338.

Morgan, P., Swanberg, C.A., 1985. On the Cenozoic uplift and tectonic stability of the Colorado Plateau. J. Geodyn. 3, 39–63.

Nakamura, D., 2009. A new formulation of garnet–clinopyroxene geothermometer based on accumulation and statistical analysis of a large experimental data set. J. Metamorph. Geol. 27, 495–508. https://doi.org/10.1111/j.1525-1314.2009.00828.x.

Needy, S.K., Anderson, J.L., Wooden, J.L., Fleck, R.J., Barth, A.P., Paterson, S.R., Memeti, V., Pignotta, G.S., 2009. Mesozoic magmatism in an upper- to middle-crustal section through the Cordilleran continental margin arc, eastern Transverse Ranges, California. In: Miller, R.B., Snoke, A.W. (Eds.), Crustal Cross Sections from the Western North American Cordillera and Elsewhere: Implications for Tectonic and Petrologic Processes. In: Geological Society of America Special Paper, vol. 456, pp. 187–218.

Porter, R., Zandt, G., McQuarrie, N., 2011. Pervasive lower-crustal seismic anisotropy in Southern California: evidence for underplated schists and active tectonics. Lithosphere 3 (3), 201–220. https://doi.org/10.1130/L126.1.

Rubatto, D., 2002. Zircon trace element geochemistry: partitioning with garnet and the link between U-Pb ages and metamorphism. Chem. Geol. 184 (1–2), 15, 123–138.

Saleeby, J.B., 2003. Segmentation of the Laramide Slab - evidence from the southern Sierra Nevada region. Geol. Soc. Am. Bull. 115, 655–668.

Saleeby, J.B., Ducea, M.N., Clemens-Knott, D., 2003. Production and loss of high-density batholithic root, southern Sierra Nevada, California. Tectonics 22. https://doi.org/10.1029/2002TC001374.

Smith, D., Arculus, R.J., Manchester, J.E., Tyner, G.N., 1994. Garnet-pyroxene-amphibole xenoliths from Chino Valley, Arizona, and implications for continental lithosphere below the Moho. J. Geophys. Res. 99 (B1), 683–696.

Smith, D., Connelly, J.N., Manser, K., Moser, D.E., Housh, T.B., McDowell, F.W., Mack, L.E., 2004. Evolution of Navajo eclogites and hydration of the mantle wedge below the Colorado Plateau, southwestern United States. Geochem. Geophys. Geosyst. 5, Q04005. https://doi.org/10.1029/2003GC000675.

Spear, F.S., 1993. Metamorphic Phase Equilibria and Pressure-Temperature-Time Paths. Mineralogical Society of America, Washington, DC, 799 pp.

Tang, M., Lee, C.-T.A., Chen, K., Erdman, M., Costin, G., Jiang, H., 2019. Nb/Ta systematics in arc magma differentiation and the role of arclogites in continent formation. Nat. Commun. 10 (1), 235. https://doi.org/10.1038/s41467-018-08198-3.

Usui, T., Nakamura, E., Kobayashi, K., Maruyama, S., Helmstaedt, H., 2003. Fate of the subducted Farallon plate inferred from eclogite xenoliths in the Colorado plateau. Geology 31 (7), 589–592.

Vetrin, V.R., Skublov, S.G., 2015. Trace elements in various genetic types of zircon from syenite of the Sakharjok massif, Kola Peninsula. Geol. Ore Depos. 58 (7), 542–550. https://doi.org/10.1134/S1075701516070126.

Watson, E.B., Wark, D.A., Thomas, J.B., 2006. Crystallization thermometers for zircon and rutile. Contrib. Mineral. Petrol., 151–413.

Wells, M.L., Hoisch, T.D., 2008. The role of mantle delamination in widespread Late Cretaceous extension and magmatism in the Cordilleran Orogen, western United States. Geol. Soc. Am. Bull. 120, 515–530. https://doi.org/10.1130/B26006.